THE ASTROPHYSICAL JOURNAL, 411:323–335, 1993 July 1

IRC +10420: A COOL HYPERGIANT NEAR THE TOP OF THE H-R DIAGRAM

TERRY JAY JONES,[1,2] ROBERTA M. HUMPHREYS,[1] ROBERT D. GEHRZ,[1] GEOFFREY F. LAWRENCE,[1,2] FRANZ-JOSEF ZICKGRAF,[3] HARVEY MOSELEY,[4] SEAN CASEY,[4] WILLIAM J. GLACCUM,[5] CAROL J. KOCH,[1] ROBERT PINA,[6] BARBARA JONES,[6] KIM VENN,[1] OTMAR STAHL,[3] AND SUMNER G. STARRFIELD[7]

Received 1992 October 5; accepted 1992 December 31

ABSTRACT

New data are reported for the OH/IR star IRC +10420, including optical/infrared imaging, spectroscopy, polarimetry, and photometry. We conclude the following:

1. The optical spectrum is that of a very luminous F supergiant (F Ia+) with a very strong O I blend at 7774 Å. Hα is strongly in emission and shows a double-peaked profile similar to the emission seen in stars with rotating equatorial disks.
2. The optical image taken through polarizing filters is elongated, and shows that the star must be intrinsically polarized at a position angle near 90°. The 8.7 μm image is also elongated, but at a position angle near 150°.
3. The optical/infrared polarization is composed of a strong interstellar component and a complex intrinsic component. The intrinsic position angle in the optical is about 100°, but rotates to about 140° in the infrared.
4. Analysis of the infrared polarization, the reddening of the optical energy distribution, and the stellar radial velocity determined from the optical spectrum indicates that IRC +10420 is at a distance of 4–6 kpc. The resulting luminosity of the star is $M_{bol} = -9.6 \pm 0.5$ mag (5 kpc), near the top of the H-R diagram at or just below the Humphreys-Davidson limit.
5. There has been a decline in the flux from the 1–7 μm continuum from the mid-1970s to the mid-1980s, whereas the optical energy distribution and the 10 μm silicate feature have remained largely unchanged over the same time period.

We propose a model for IRC +10420 in which a true core-burning supergiant is surrounded by a rotating equatorial disk of gas and dust that is viewed from about midway above the plane. Dissipation of dust near the star is responsible for the drop in the infrared continuum. The polarization and OH emission are caused by a complex distribution of gas and dust that surrounds the star and its disk from an earlier phase of evolution. IRC +10420 may be evolving from a red supergiant to the blue side of the H-R diagram, perhaps to become a Wolf-Rayet star. We argue that it is now in a phase of evolution that is analogous to that of degenerate core giants evolving through the proto–planetary nebula phase, but at a much higher luminosity.

Subject headings: polarization — stars: evolution — stars: individual (IRC +10420) — stars: supergiants

1. INTRODUCTION

IRC +10420 has the visible spectrum of a very luminous F supergiant (F8 Ia+) and a very large infrared excess from circumstellar dust (Humphreys et al. 1973). A very high mass-loss rate of $3 \times 10^{-4}\ M_\odot\ \mathrm{yr}^{-1}$ has been estimated from its CO emission (Knapp & Morris 1985), assuming a distance of 3.4 kpc. It also shows strong OH maser emission, and with spectral type F, the star is one of the warmest stellar OH masers known (Giguere, Woolf, & Weber 1976). IRC +10420 shows considerable variability in OH line emission and has also brightened in the visual by about 1 mag from 1930 to 1970 (Gottlieb & Liller 1978).

The OH maser emission from IRC +10420 has been extensively studied by several authors (Nedoluha & Bowers 1992; Lewis, Terzian, & Eder 1986; Diamond, Norris, & Booth 1983) and shows emission at 1612, 1665, and 1667 MHz. The emission is unusual in that it emanates from a region surrounding a relatively warm star in comparison with the cooler, classic red giant and supergiant stellar masers. The 1667 MHz emission extends over a larger angular region than the 1612 MHz emission (Bowers 1984). Recent observations show that the 1612 MHz satellite emission has increased substantially, while the main line 1665 emission has weakened (Lewis et al. 1986). There is also substantial circular polarization in the OH lines (Reid et al. 1979), indicating significant magnetic fields of 1–10 mG. The spatial distribution of the OH maser emission is very complex, clumpy, and a strong function of maser velocity (Nedoluha & Bowers 1992).

Although the nature of IRC +10420 is still unclear, many authors have included the star in the loosely defined "proto–planetary nebula" classification (e.g., Habing, Hekkert, & van der Veen 1989; Hrivnak, Kwok, & Volk 1989; Johnson & Jones 1991; Bowers & Knapp 1989). These are stars with $L \leq 10^4\ L_\odot$ that have recently left a high mass-loss phase on

[1] Department of Astronomy, University of Minnesota, 116 Church Street, S.E., Minneapolis, MN 55455.
[2] Guest Observer, Infrared Telescope Facility, operated by the University of Hawaii under contract with NASA.
[3] Landessternwarte, Heidelberg-Königstuhl, D-6900 Heidelberg 1, Germany.
[4] Laboratory for Astronomy and Astrophysics, Goddard Space Flight Center, Greenbelt, MD 20771.
[5] Space Science Division, Naval Research Laboratory, 4555 Overlook Avenue, S.W., Washington, D.C., 20375.
[6] Center for Astrophysics and Space Science, Code 0111, University of California at San Diego, La Jolla, CA 92093.
[7] Department of Physics and Astronomy, Arizona State University, Tempe, AZ 85287.

the upper asymptotic giant branch (AGB) and are now evolving toward the planetary nebula stage. The very low surface gravity in their tenuous photospheres produces a supergiant spectrum, even though their higher latitude distribution indicates that these stars are not true supergiants with massive main-sequence progenitors. Classic examples include 89 Her and the Egg Nebula.

Other investigators have treated IRC +10420 as a true supergiant (Humphreys et al. 1973; Giguere et al. 1976; Mutel et al. 1979). Estimates of its distance have ranged from 3 to 7 kpc, depending on which observations and assumptions have been given the most weight. Any distance larger than 1 kpc places IRC +10420 above the luminosity of typical proto–planetary nebulae. In fact, any distance greater than 3 kpc places the star above the AGB limit, the upper limit in luminosity for degenerate core giants.

Speculation on the evolutionary status of IRC +10420 has been limited. Humphreys et al. (1973) initially compared IRC +10420 with η Carinae, based on the similarities in energy distribution and its high luminosity. Mutel et al. (1979) suggested that the dust shell around the star could have been formed in a previous evolutionary phase, probably when the star was a red supergiant. They suggested that the mass loss has stopped and that the remaining "fossil" shell should dissipate with time. In this paper we present an extensive set of new observations that include optical imaging, spectroscopy, photometry, and polarimetry and infrared imaging, photometry, and polarimetry. These observations show that IRC +10420 is among the most luminous hypergiants known. The spectral similarities to the proto–planetary nebulae can be understood if IRC +10420 is evolving into a hotter star from a cool supergiant that experienced a high mass loss in a manner analogous to, but at a very much higher luminosity than, the proto–planetary nebulae.

2. OBSERVATIONS

2.1. *Optical*

We obtained an echellette spectrum covering the range 3900–10250 Å with a resolution between 1 and 2 Å with the Cassegrain spectrograph and cross-disperser on the 3.5 m telescope at Calar Alto. Several exposures were made, ranging from 120 to 1800 s. An Hα spectrum was made at a resolution of 0.5 Å with the coudé spectrograph on the 2.2 m telescope, also at Calar Alto in 1988 September. The Hα spectrum and portions of the moderate-resolution spectrum are shown in Figures 1 and 2.

Optical images of IRC +10420 were obtained using photographic plates taken by E. P. Ney in 1976 with the Palomar 48 inch (1.2 m) Schmidt telescope. These plates were taken through a polarizing sheet at both a north-south and an east-west orientation. They were subsequently scanned and digitized using the University of Minnesota's automated plate scanner in isodensitometry mode with four thresholds. The contours for the next to lowest threshold are shown in Figure 3 for both orientations of the polarizer. The image taken in polarized light at a position angle of 180° (polarizer oriented north-south) is round. The image taken in polarized light at a position angle of 90° is clearly extended north-south, while the images of other stars in the field are round.

Optical photometry of IRC +10420 in the Cousins-Kron (CK) *B*, *V*, *R*, and *I* passbands was done on 1991 October 16 at the UM/UCSD 1.5 m at Mount Lemmon Observatory using the Two-Holer Photopolarimeter (Sitko, Schmidt, & Stein 1985). Standard stars were chosen from the list compiled by Landolt (1983). Mean extinction coefficients were assumed, as were transformation coefficients between the instrumental Two-Holer system and the CK system. The results are given in Table 1.

Optical polarimetry in the CK *V*, *R*, and *I* passbands was done on 1991 October 16, also at the UM/UCSD 1.5 m telescope at Mount Lemmon Observatory using the Two-Holer Photopolarimeter and a 8″.3 aperture. Instrument efficiency and calibration of the position angle were checked using published values for stars with large interstellar polarization. The results are given in Table 2, where the errors are $\pm 1\ \sigma$.

2.2. *Infrared*

We accumulated photometric observations of IRC +10420 over a 20 yr baseline from 1972 through 1992 using optical/infrared photometers at the University of Minnesota (UM) O'Brien Observatory (OBRIEN; 76 cm telescope, 29″ diaphragm), The UM/UCSD Mount Lemmon Observing

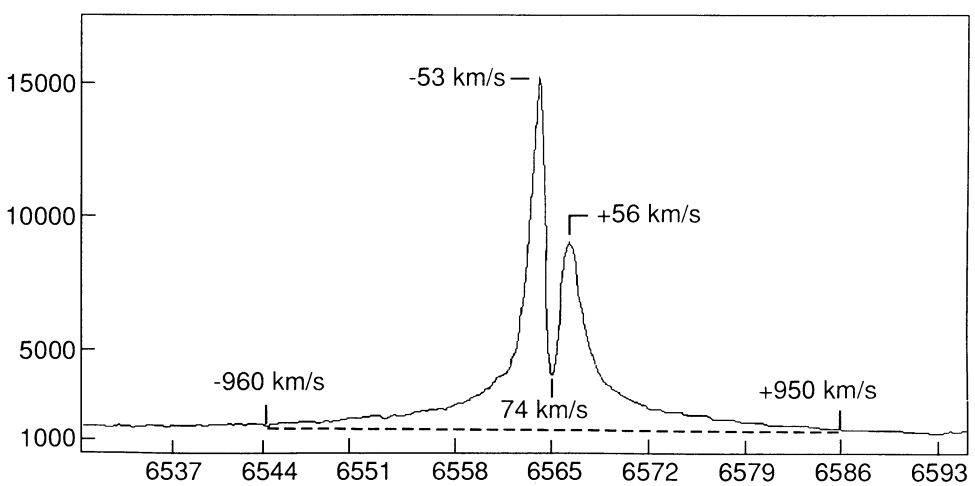

FIG. 1.—Hα spectrum of IRC +10420. Note the double-peaked emission profile with the central reversal centered at the radial velocity of the star. Also note the high-velocity wings. The central absorption velocity is with respect to the LSR.

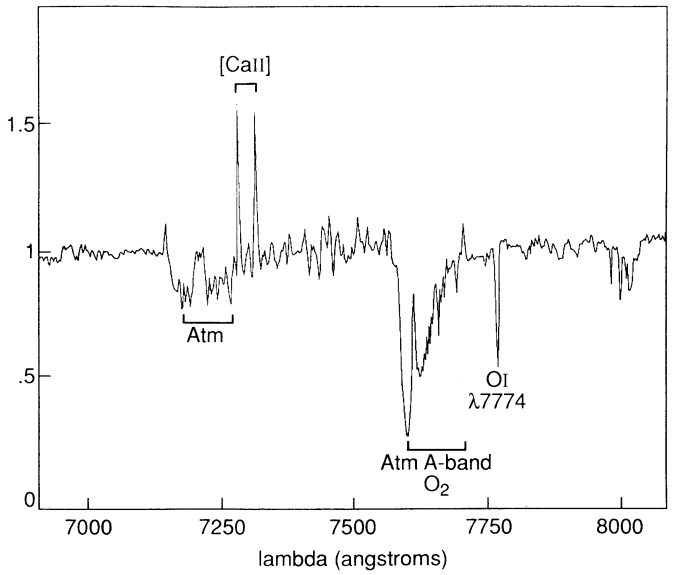

FIG. 2a

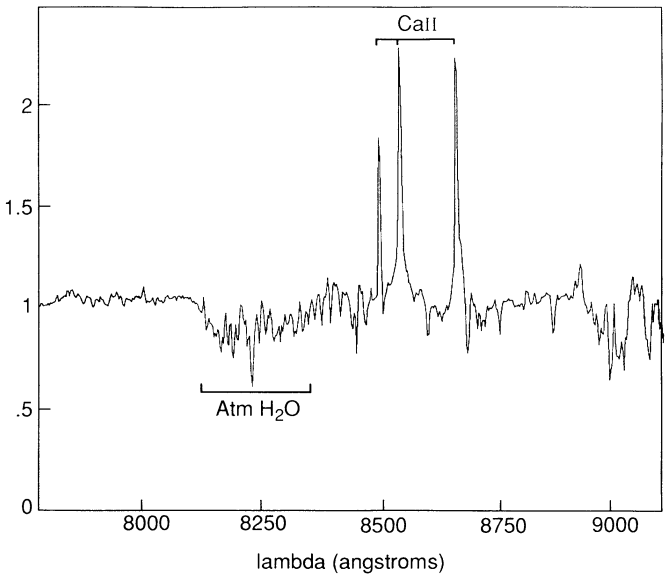

FIG. 2b

FIG. 2.—(*a*) Portion of the spectrum of IRC +10420 showing the O I photospheric line at 7774 Å and the [Ca II] lines near 7300 Å. (*b*) Portion of the spectrum of IRC +10420 showing the Ca II triplet near 8500 Å.

Facility (MLOF; 152 cm telescope, 10″ diaphragm), the Wyoming Infrared Observatory (WIRO; 234 cm telescope, 5″ diaphragm), and the NASA IRTF (3 m telescope, 6″ diaphragm). Our photometric observations are summarized in Table 1, along with all of the known photometric data (except the narrow-band photometry of Craine et al. 1976) obtained on IRC +10420 since its discovery during the Caltech 2 Micron All-Sky Survey in 1965 by Neugebauer & Leighton (1969). The diaphragm sizes were, in all cases, large enough to encircle the flux from the extended IRC +10420 nebula (§ 3.5), although this condition was only marginally met by the 5″ WIRO diaphragm. Our observations used throws large enough so that the reference beams were not contaminated by the extended nebula.

The effective wavelengths and calibration of the OBRIEN system were described by Humphreys et al. (1973) and Ney (1974), and a similar description of the photometric system used at MLOF was given by Hanner et al. (1990) and Lawrence, Jones, & Gehrz (1990). Gehrz & Hackwell (1978) described operations at WIRO, and the Wyoming photometric system effective bandpasses and calibration were characterized by Gehrz, Hackwell, & Jones (1974) and Gehrz, Grasdalen, & Hackwell (1987). The IRTF system and its transformation to other systems is described in Humphreys, Jones, & Sitko (1984). The energy distribution of IRC +10420 at two different epochs is shown in Figure 4.

We obtained 16–30 μm spectrophotometry of IRC +10420 on 1991 June 28 UT using the Goddard Space Flight Center 24 channel spectrophotometer (Omont et al. 1990) on the 76 cm telescope of the NASA Kuiper Airborne Observatory (KAO) flying at an altitude of 41,000 feet (12.5 km). The instrument

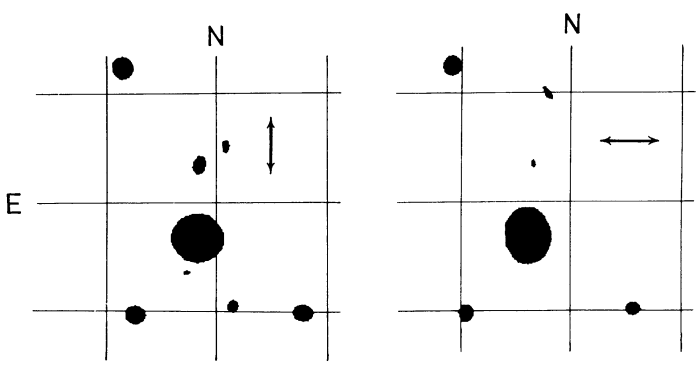

FIG. 3.—Isodensity contours of photographic images of IRC +10420 and its immediate vicinity taken through a polarizing filter. The image in the left-hand panel was taken with the polarizer oriented (electric vector) north-south. The image in the right-hand panel was taken with the polarizer oriented east-west. Note the elongation of the image with the east-west orientation of the polarizer.

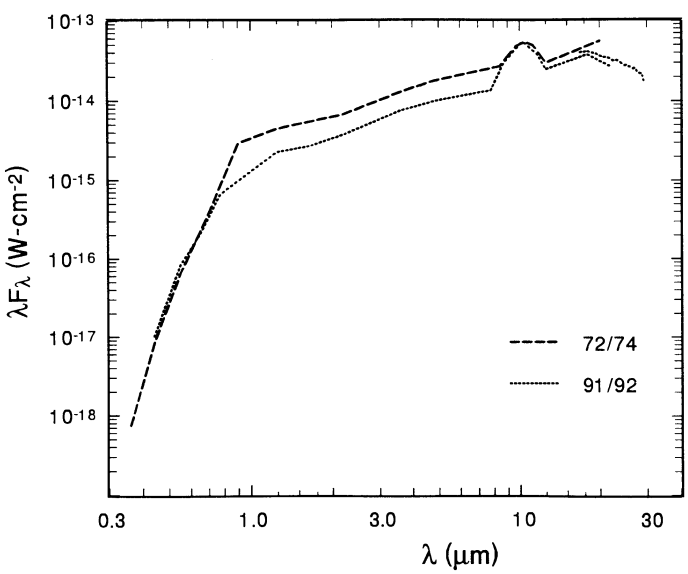

FIG. 4.—The 0.3–30 μm energy distribution of IRC +10420 at two different epochs. Note the strong 1–5 μm continuum and the heavily reddened visual continuum.

TABLE 1

PHOTOMETRIC HISTORY OF IRC +10420

A. INFRARED

Bandpass				J	H	K	L	M	7μm	8μm	9μm	10μm	11μm	12μm	19μm	20μm
Wavelength (μm)				1.25	1.60	2.2	3.4	4.0	7.8	8.4	9.7	10.3	11.0	12.0	18.0	20
					(1.65)	(2.25)	(3.45)	(4.8)		(8.6)	(9.8)	(10.5)	(11.2)	(12.2)	(19.5)	(21)
						[2.30]	[3.50]	[4.9]		[8.7]	[10.0]	[10.7]	[11.4]	[12.5]		[22]
							{3.58}	{5.0}		{8.8}			{11.6}	{12.6}		{23}
							/3.60/									/25/
							'3.80'									
UT Date	JD 2440000+	Source, Observer †	Facility #													
1965/1966	-	(1)	CIT	-	-	[+2.75]	-	-	-	-	-	-	-	-	-	-
1971 Apr 3	1045	(2)	AFGL	-	-	-	-	-	-	-	-	-	-4.2	-		-6.60
1972 Sep 9	1570	(3)	OBRIEN	-	-	[+2.70]	+0.65	(-0.65)	-	(-3.35)	-	[-4.45]	-	(-4.65)	-	-
1972 Oct 16	1607	RDG,JAH	KPNO	-	-	[+2.67]	/+0.50/	[-0.81]	-	[-3.02]	-	-	[-4.74]	{-4.86}	(-6.41)	(-6.74)
1972 Oct 16	1607	RDG,JAH	KPNO	-	-	-	-	-	-	-	-	-	-	-	-	{-6.76}
1973 Jul 29	1893	(5)	SSO	-	-	+2.75	/+0.61/	(-0.58)	-	-2.81	-3.88	(-4.25)	(-4.34)	[-4.13]	-	-6.44
1974 Jul 27	2256	(6)	OBRIEN	+4.8	(+3.70)	(+2.60)	{+0.40}	[-0.80]	-	(-3.40)	-	[-4.60]	-	(-4.10)	-	-
1974 Nov 8	2360	(6)	OBRIEN	+4.80	(+3.70)	(+2.60)	{+0.60}	[-0.60]	-	(-3.20)	-	[-4.60]	-	(-4.70)	-6.40	-
1977 Sep 1	3388	(6)	OBRIEN	+5.20	(+3.80)	(+2.90)	{+0.90}	[-0.20]	-	(-3.00)	-	[-4.40]	-	(-4.00)	-	-
1980 Jul 6	4427	(7)	WIRO	-	-	[+2.96]	/+0.84/	[-0.60]	-	[-2.88]	[-3.80]	-	[-4.40]	(-4.39)	(-5.70)	-
1983 May	5472	(8)	UKIRT	-	-	+3.40	'+0.80'	(-0.20)	-	-	-	-	-	-	-	-
1983	-	(9)	IRAS	-	-	-	-	-	-	-	-	-	-	-4.19	-	/-6.34/
1991 Mar 8	8324	RDG,GFL,RO	MLOF	+5.54	+4.59	+3.39	-	[-0.90]	-1.80	[-2.99]	(-3.85)	-4.14	{-4.15}	[-3.89]	-5.61	[-5.87]
1991 Sep 1	8501	GFL	OBRIEN	-	+4.56	-	/+1.14/	[-0.03]	-	-	-	-	-	-	-	-
1991 Sep 4	8504	GFL	OBRIEN	-	-	-	-	-	-2.00	[-2.97]	(-3.80)	-	{-4.32}	[-4.06]	-	-
1991 Sep 16	8516	TJJ,GFL	IRTF	-	-	+3.47	(+1.36)	{-0.02}	-1.80	[-3.09]	(-3.89)	-4.02	{-4.31}	[-4.30]	-	-5.95
1992 Mar 12	8694	RDG,TJJ	OBRIEN	+5.28	+4.39	[+3.29]	/+1.24/	[-0.11]	-2.03	[-3.07]	(-3.87)	-4.07	(-4.33)	[-4.12]	-5.94	-
1992 Apr 12	8725	RDG	OBRIEN	+5.06	+4.32	[+3.19]	/+1.18/	[-0.18]	-	-	-	-4.14	-	-	-	-

B. ULTRAVIOLET AND VISUAL

Bandpass				U	B	V	R	I
Wavelength (μm)				0.36	0.44	0.55	0.65	0.77
							(0.70)	(0.84)
								[0.90]
UT Date	JD 2440000+	Source, Observer †	Facility #					
1965/1966	-	(1)	CIT	-	-	-	-	(+8.00)
1972 Oct 4	1595	(4)	STEW	+15.70	+13.80	+11.10	(+8.70)	[+6.00]
1972 Oct 7	1598	(3)	OBRIEN	-	+14.00	+11.30	-	-
1991 Oct 16	8546	TJJ,GFL	MLOF	-	-	+10.93	+9.56	+7.95

† Observers: R. D. Gehrz (RDG), J. A. Hackwell (JAH), T. J. Jones (TJJ), G. F. Lawrence (GFL), and R. Olson (RO). Other data taken from (1) Neugebauer & Leighton 1969; (2) Walker & Price 1975; (3) Humphreys et al. 1973; (4) Lee 1972; (5) Thomas, Robinson, & Hyland 1976; (6) Ney & Merrill 1980; (7) Grasdalen et al. 1983; (8) Dyck et al. 1984; (9) *IRAS* Point Source Catalog, Version 2 1988.

Facilities are the Caltech Two Micron Survey Telescope (CIT), the Air Force Geophysical Laboratory All Sky Survey (AFGL), University of Minnesota O'Brien Observatory (OBRIEN), Steward Observatory (STEW), Kitt Peak National Observatory (KPNO), Siding Spring Observatory (SSO), Wyoming Infrared Observatory (WIRO), United Kingdom Infrared Telescope (UKIRT), NASA Infrared Telescope Facility (IRTF), and UM/UCSD Mount Lemmon Observing Facility (MLOF).

TABLE 2

POLARIMETRY

Passband	P (%)	θ
B (0.44 μm)	0.7 ± 0.32	(174°) ...
V (0.55 μm)	1.42 ± 0.07	168.6 ± 2
R (0.65 μm)	1.98 ± 0.05	174.1 ± 1
I (0.77 μm)	2.36 ± 0.05	174.8 ± 1
J (1.22 μm)	2.20 ± 0.10	172 ± 2
H (1.65 μm)	1.53 ± 0.05	163 ± 2
K (2.2 μm)	0.90 ± 0.10	166 ± 3
L (3.6 μm)	0.86 ± 0.10	151 ± 3

was configured to have a 0.5 μm spectral bandwidth, and the diaphragm size was 30″. The reference beam as 60″ from the source beam in azimuth. Arcturus (α Boo) was the primary calibrator, and Ras Algethi (α Her) was observed for comparison. Glaccum et al. (1987) presented a detailed discussion of the data reduction procedures. Our KAO data are summarized in Table 3 and Figure 5. We have also shown for comparison in Figure 5 the mean of two additional 10–30 μm spectra obtained with the KAO in 1976 May and 1978 May by Forrest, McCarthy, & Houck (1979). Spectrophotometry through the silicate feature in the 10 μm band is reported in Giguere et al. (1976) and in the *Infrared Astronomical Satellite* Atlas of Low Resolution *IRAS* Spectra 1986).

Images at 8.7 μm ($\Delta\lambda = 1$ μm) were obtained using the Golden Gopher array camera on 1991 October 14 at the UM/UCSD 1.5 m telescope at Mount Lemmon Observatory. This camera contains an Aerojet 20 × 64 SiAs impurity band detector array with a useful wavelength range of 5–27 μm. The camera electronics were built at UCSD and intercept 16 of the 20 data lines from the direct readout array, making an effective 16 × 64 element array. The image scale on the 1.5 m telescope is 0.″83 pixel^{-1}. Images of α Her were used for photometric calibration, and images of μ UMa were used to determine the point-spread function (there was no offset guide star available for α Her). The images of μ UMa had a full width at half-maximum of 2.″0. The flux-calibrated image of IRC +1042 is shown in Figure 6 and is clearly extended relative to the images of μ UMa.

Infrared polarimetric observations were made on 1991 September 17 and 19 on the IRTF through a 6″ aperture using the Minnesota Infrared Polarimeter (MIRP; Jones & Klebe 1988). Polarimetry was done in the J (1.22 μm), H (1.65 μm), and K (2.2 μm) passbands and through an L-band filter centered at 3.6 μm. Instrument efficiency and position-angle calibration were checked using published values for stars with large interstellar polarization. Position-angle calibration at 3.6 μm was done using W33A. The results are given in Table 2, where the errors are ±1 σ.

TABLE 3

KAO SPECTROPHOTOMETRY

Wavelength (μm)	F_λ (10^{-15} W cm^{-2} μm^{-1})
16.86	2.40 ± 0.04
18.13	2.29 ± 0.02
18.78	2.21 ± 0.02
19.43	2.00 ± 0.02
20.00	1.84 ± 0.01
21.25	1.65 ± 0.02
21.86	1.56 ± 0.02
22.45	1.42 ± 0.05
23.07	1.38 ± 0.02
23.64	1.34 ± 0.02
24.25	1.20 ± 0.02
24.80	1.12 ± 0.02
25.39	1.10 ± 0.02
25.93	1.03 ± 0.01
26.44	0.95 ± 0.02
27.16	0.94 ± 0.04
27.63	0.83 ± 0.02
25.16	0.79 ± 0.03
28.69	0.77 ± 0.01
29.17	0.61 ± 0.02

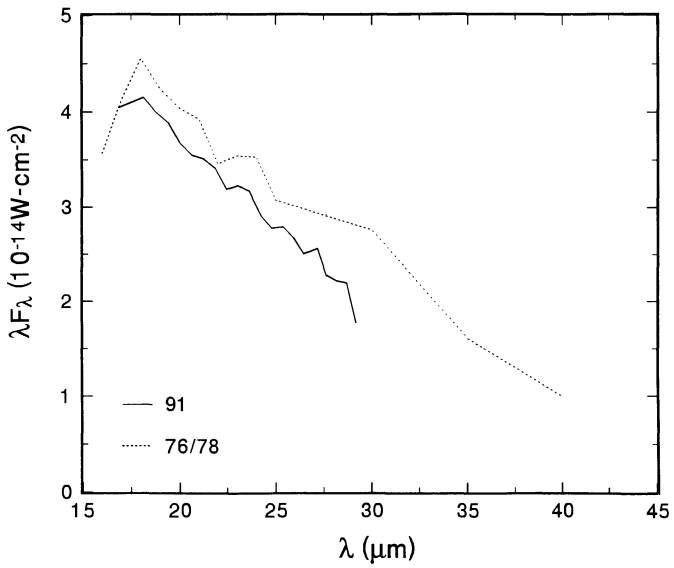

FIG. 5.—The 20 μm spectrum of IRC +10420 taken in 1991 with the GSFC spectrometer on the KAO (*solid line*; Table 3). The dashed line is the average of two spectra from 1976 and 1978 reported in Forrest et al. (1979).

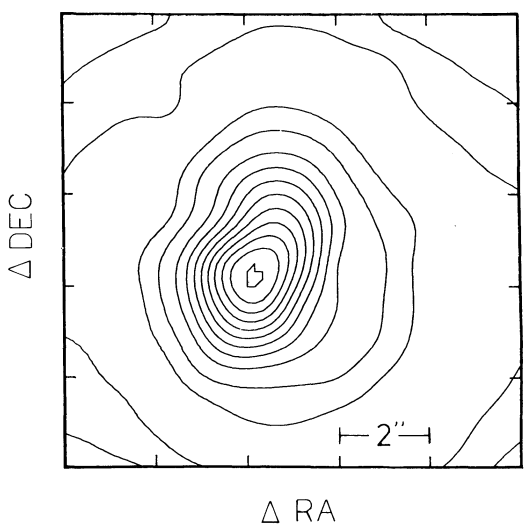

FIG. 6.—Image of IRC +10420 at 8.7 μm taken with the UCSD Golden Gopher array camera. The extension of the image to the northwest is real. The main peak to the southeast is consistent with the point-spread function for stars observed before and after this image was taken.

3. ANALYSIS

3.1. *Optical Spectrum.*

The echellette spectrum covering the wavelength range 3900–10250 Å shows sharp, strong absorption lines of a very luminous F-type supergiant. The O I blend at 7774 Å (Fig. 2*a*), a very posttive luminosity indicator (Osmer 1972a, b; Slovik & Peterson 1992; Peterson 1992), is extremely strong in IRC +10420. With a measured equivalent width of 3.5 Å, it is off the top of the W_λ versus M_V relation that is calibrated up to $M_V \sim -9$ mag (Slovik & Peterson 1992). Extrapolating this calibration would imply an absolute visual magnitude of at least $M_V = -10$ mag. The extremely strong O I feature certainly implies a very low surface gravity for IRC +10420.

The spectrum also shows several emission lines. The identified emission lines are listed in Table 4. The most prominent and most interesting are the dual-peaked Hα profile (Fig. 1), the strong emission in the Ca II triplet near 8500 Å (Fig. 2*b*), and the [Ca II] lines near 7300 Å (Fig. 2*a*). The Ca II triplet emission is probably produced in the very extended atmosphere by radiative de-excitation from the absorption by the strong Ca II H and K lines in the star's photosphere. The forbidden Ca II lines are rarely seen. They were first reported in the peculiar hydrogen-deficient star υ Sgr by Merrill (1943), and are also found in the spectra of some symbiotic stars (Andrillat 1982). The transition that produces the Ca II "infrared" triplet emission lines leaves the atoms in the upper level for the forbidden lines. These atoms are normally collisionally de-excited back to the ground state that produces the H and K lines. We can estimate the relative number of photons that are radiatively de-excited to produce the observed forbidden lines by multiplying the expected continuum fluxes at 7300 and 8600 Å by the combined equivalent widths of the [Ca II] and Ca II lines, respectively. We find that about one-fourth of the photons are producing the forbidden lines by radiative de-excitation to the ground state, and the electron density is therefore about 3 times higher than the critical density for complete radiative decay. Thus the [Ca II] lines are produced in a region of much lower density than is normally found even in the atmospheres of the most luminous F- and G-type supergiants.

The Hα profile from the coudé spectrum (Fig. 1) looks very much like that for a rotating disk, similar to the Hα emission in classical Be stars The absorption dip has the same velocity as the absorption lines in the F supergiant spectrum suggesting that it arises at least partly in the photosphere and that the disk is not moving radially to any significant extent. The two emission components are symmetrically displaced at −53 and +56 km s^{-1}, implying a rotation velocity of 50–60 km s^{-1} for the disk.

TABLE 4

IDENTIFIED EMISSION LINES IN IRC +10420

Hα	Fe II λ7711
Hβ	Fe II λ6516
	Fe II λ6432
Ca II λ8662	Fe II λ6417
Ca II λ8542	Fe II λ6238
Ca II λ8489	Fe II λ6148
	Fe II λ6084
[Ca II] λ7323	Fe II λ5911
[Ca II] λ7291	
[S II] λ6719	[Fe II] λ7157

The very broad wings on the Hα profile are unusual and extend to ±800–900 km s^{-1} or more. They might be produced in a higher velocity and more symmetrical mass outflow at a much larger distance from the star. Some of the Hα wings may be due to electron scattering of Hα photons in the rotating disk, similar to the process seen in classical Be stars (Doazan 1982) and B[e] supergiants (Zickgraf et al. 1985, 1986). The wings are too broad to be explained solely by this mechanism, however, since the scattering disk is rotating at only 50–60 km s^{-1}.

We have measured the velocity of IRC +10420 from both the absorption and the emission lines. The absorption lines used include the Paschen series in the far-red, the strong O I 7774 Å line, and several metallic lines in the red coudé spectrum. The velocity is 78.7 ± 0.9 km s^{-1} (LSR). The emission lines of Fe II and [Fe II] in the red spectrum and the pair of [Ca II] lines give an LSR velocity of 76.2 ± 1.1 km s^{-1}. These velocities disagree with the velocity for the absorption lines of 97 km s^{-1} reported by Fix (1981) and Fix & Cobb (1987). However, our velocities from the absorption and emission lines from both the coudé and echellette spectra are consistent with each other and with the LSR velocity of 75 km s^{-1} often quoted for IRC +10420, based on the midpoint of the OH maser emission (Giguere et al. 1976; Bowers 1984). In agreement with Fix (1981), we also find that the Na I D lines have a velocity blueshifted by about 40 km s^{-1} relative to the star and which we also attribute to a strong interstellar component.

3.2. *Polarimetry*

Our new polarimetry together with the polarimetry from Craine et al. (1976) is shown in Figure 7. The polarization has clearly changed since 1975, and the wavelength dependence of the polarization and position angle shows a complicated mixture of polarization mechanisms. The relatively broad peak in wavelength dependence of the polarization centered in the mid-visual at a position angle close to 180° indicates a substantial contribution from interstellar polarization at roughly this position angle. The optical image is extended north-south in light polarized at a position angle of 90° (§ 2.1), very different from the ∼180° position angle seen in the single-aperture polarimetry. Since interstellar polarization cannot spread out the image on the sky, this strongly suggests that the object is extended and the intrinsic polarization is at a position angle close to 90°. The bulk of the polarization in the mid-visual is therefore interstellar. Craine et al. (1976) made an estimate of the interstellar component by fixing the position angle for the interstellar polarization at 180°, based on polarimetry of stars close to IRC +10420 in the sky. They then varied P_{max} and λ_{max} for the interstellar component to obtain a minimum in the intrinsic polarization after vector subtraction. Their estimate for the interstellar polarization was a very substantial 12% (P_{max}), which demands that the interstellar extinction is *at least* $A_V = 4$ mag, and more likely $A_V \sim 6$–7 mag (Serkowski, Mathewson, & Ford 1975).

In general, both interstellar and circumstellar polarization decrease at wavelengths longer than 1 μm (e.g., Wilking et al. 1980; McCall & Hough 1980; Johnson & Jones 1991). For simple single scattering in dust shells around red giants, circumstellar polarization drops faster into the red and infrared than does interstellar polarization (Dyck, Forbes, & Shawl 1971; Johnson & Jones 1991). This suggests that the *I*, *J*, *H*, and *K* band polarization of IRC +10420 is most strongly influenced by the interstellar component and can provide a

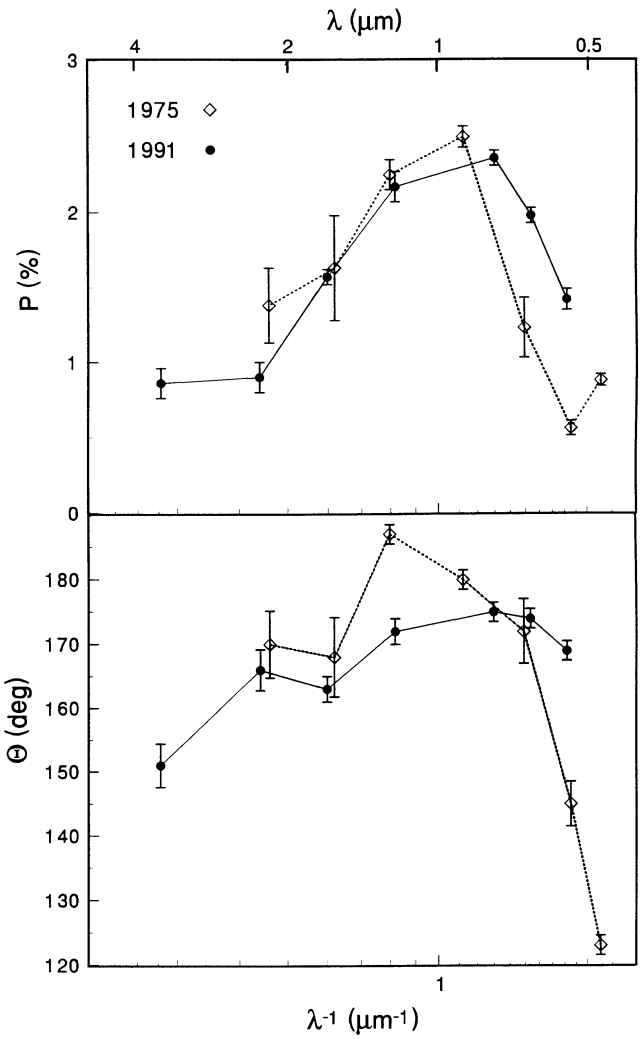

FIG. 7.—Observed percent polarization (*upper panel*) and position angle (*lower panel*) for IRC +10420. The 1991 data are from Table 2. The 1975 data are from Craine et al. (1976). Note the complicated wavelength dependence of the position angle.

rough estimate of the magnitude of the interstellar polarization independent of any assumptions about the intrinsic component or interstellar extinction. An assumed interstellar component can be vector-subtracted from the observed polarization and an estimate of the intrinsic component obtained. Often, the additional constraint of requiring no rotation in position angle for the resulting intrinsic polarization is applied to this process (e.g., Jones & Gehrz 1990). We tried this approach, but were successful only when a very large (20% or more) interstellar polarization was used. The polarization of IRC +10420 is sufficiently complex that it became obvious that the intrinsic component shows a rotation in position angle.

The average position angle of the two most highly polarized stars near IRC +10420 (HD 183143 and HD 183888) is about 10°, so we will use this position angle for the interstellar component. Using $P_{K\text{inter}} = 1.5\%$ for the interstellar polarization at K, and extrapolating to the visual via the standard extended Serkowski relation from Wilking et al. (1980) with $\lambda_{\max} = 0.55$ μm, we obtain the intrinsic polarization plotted in Figure 8. Because of the uncertainy in the value of the interstellar polarization, the values for polarization and position angle of the calculated intrinsic component are highly uncertain. Two features of the calculated intrinsic polarization, however, were always present for a very wide range of choices for the interstellar component. The first is the general decline in intrinsic polarization from the blue to the red and infrared. This is very common behavior in dusty stars (e.g., Dyck et al. 1971). The second is the rotation in position angle from the blue to the red. The calculated position angle in the visual is about 100°, in good agreement with the north-south extension of the visual image of IRC +10420 when viewed in light polarized at 90° (§ 2.1).

3.3. *Distance and Luminosity*

Our interpretation of the data and our understanding of IRC +10420 will depend on its intrinsic luminosity and therefore its distance. With a $B-V$ color of 2.7 mag [$E(B-V) \sim 2.2$.], IRC +10420 is very highly reddened, but it is uncertain how much of this reddening is interstellar and how much is circumstellar. If all of the $B-V$ color excess is inter-

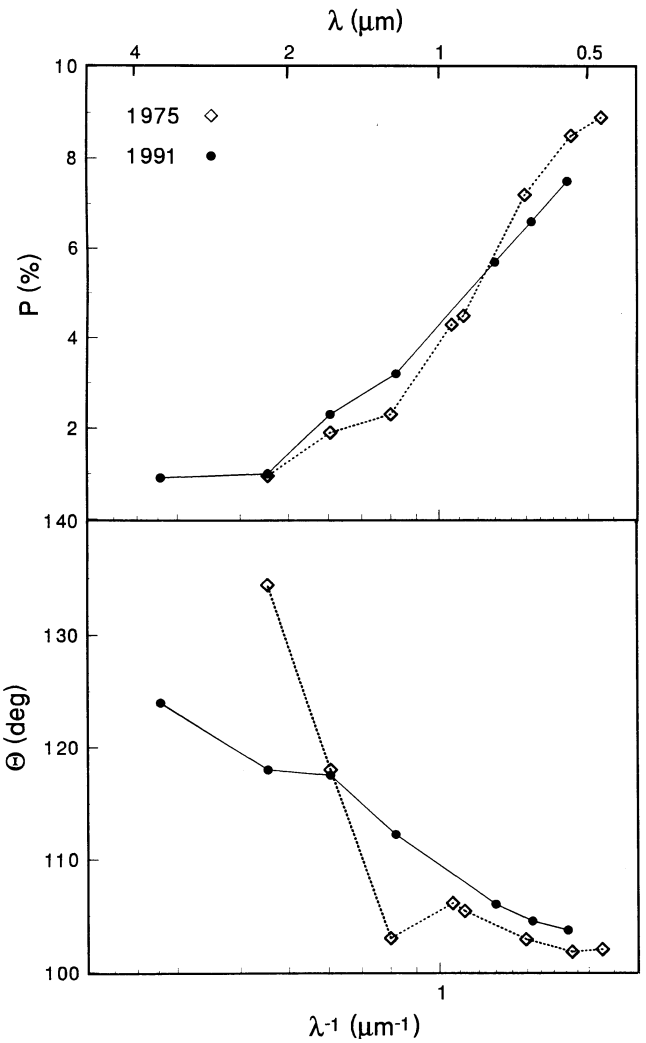

FIG. 8.—Intrinsic polarization for IRC +10420 after removal of the interstellar component. The percent polarization (*upper panel*) and position angle (*lower panel*) are shown for both the recent observations (Table 2) and the observations in 1975 from Craine et al. (1976). Note the rotation in position angle from the visual to the infrared.

stellar, then the interstellar extinction is $A_V \sim 6.5$ mag. Both our analysis of the polarization data and the analysis by Craine et al. (1976) show that there is considerable interstellar polarization in IRC +10420. The observed level of interstellar polarization demands a corresponding amount of interstellar extinction, very likely $A_V = 6$–7 mag. Although the large infrared excess in IRC +10420 indicates significant circumstellar dust around the star, a tilted disk geometry would provide a natural way for us to view the photosphere of the star through only a modest ($A_V \sim 1$) circumstellar extinction at most. The remaining major fraction of the extinction would then be interstellar.

The interstellar extinction of other stars in the direction of IRC +10420 ($l = 47°$, $b = -2.5°$) is observed to increase significantly up to $A_V = 4$ mag at distances of 3–4 kpc (see also Craine et al. 1976). Therefore, IRC +10420 must be more than 4 kpc from the Sun. Its kinematic distance also indicates that IRC +10420 is a large distance from the Sun (see Giguere et al. 1976). In the direction of IRC +10420 the radial velocity at the tangent point is about 65 km s^{-1} (Clemens 1985). The velocity midpoint of the OH maser spectrum is +75 km s^{-1} (Giguere et al. 1976), very close to the stellar radial velocity we derived from the optical spectra. The maximum observed H I velocity in this direction is also 75 km s^{-1}. IRC +10420 is probably associated with this feature, and assuming that this maximum velocity occurs at the tangent point leads to a distance of 5.8 kpc ($R_0 = 8.5$ kpc) from the Sun. The presence of interstellar Na D lines in the spectrum at a velocity blueshifted with respect to the stellar velocity (Fix 1981, § 3.1) is in accordance with this conclusion.

Integrating the energy distribution (see Fig. 4) from 0.5 to 25 μm (corrrected for an interstellar extinction of $A_V = 6$ mag) gives $M_{bol} = -9.1$ to -10.0 mag for a distance range of 4–6 kpc. Since the bulk of the flux is at infrared wavelengths, the correction for extinction has only a modest effect. The derived luminosity is consistent with the spectrum of the star (§ 3.1) and places IRC +10420 very far above the luminosity of proto–planetary nebulae and well above the AGB limit, the maximum luminosity possible for red giants with low- to intermediate-mass main-sequence progenitors. If IRC +10420 were a typical proto–planetary nebula star with a luminosity of $\sim 10^4\ L_\odot$, it would be at a distance of only 600 pc, which is inconsistent with the observed interstellar polarization, the radial velocity, and the interstellar sodium absorption lines.

3.4. *Photometric History*

The long-term infrared photometric temporal development of IRC +10420 since its discovery in 1965 is summarized in Table 1 and Figures 4, 9 and 10. The optical light curve is given by Gottlieb & Liller (1978). Figure 4 shows the 0.3–30 μm energy distribution of IRC+10420 as it appeared in the early 1970s compared with its appearance in recent years. Figures 9 and 10 show the light curves of IRC +10420 at several infrared wavelengths. We are able to identify several trends that characterize the long-term temporal development of the energy distribution of IRC +10420.

Gottlieb & Liller (1978) show that from 1926/1927 to 1970, IRC +10420 slowly and steadily brightened by about 1 mag in the blue. For the past 20 yr our measurements (Humphreys et al. 1973, Table 1) are consistent with the interpretation that the visual flux from IRC +10420 has remained essentially constant at $V \sim 11.1 \pm 0.2$ mag. The narrow-band optical photometry reported by Craine et al. (1976) for 1974 August 8–15 is in close agreement with our broad-band photometry.

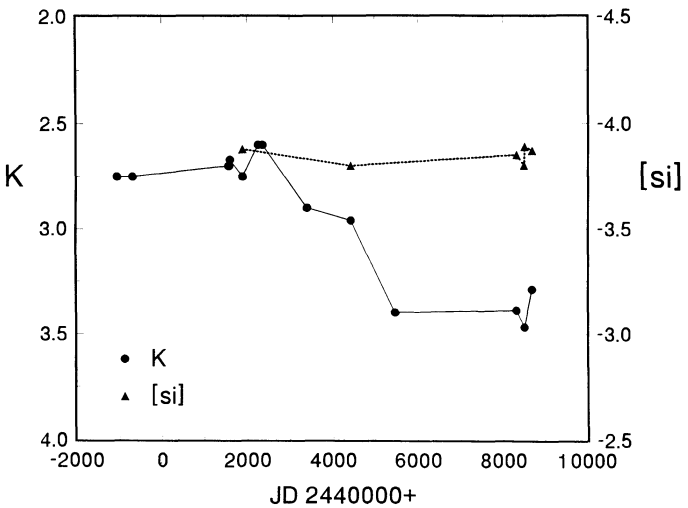

FIG. 9.—Photometric light curve of IRC +10420 from 1965 to 1992 at K (2.2 μm) and in the center of the silicate emission feature (column labeled 10 μm in Table 1). The 2 μm continuum has sharply declined since the mid-1970s, but the 10 μm silicate emission feature has remained relatively constant.

The infrared continuum from 1 to 7.5 μm, which has a slope of $\lambda^{1.3}$ in λF_λ, has dropped about 1.3 mag (a factor of 3.3) since 1972 (see Fig. 4). The infrared light curves (K band; Figs. 9 and 10) show that this drop occurred rather steadily during the 6 yr period from 1974 to 1980 following an apparent brightening in 1974. The slope of the near-infrared continuum has remained remarkably constant.

The strength of the 10 μm silicate emission feature as measured with narrow-band filters (column labeled 9 μm in Table 1; Fig. 9) has remained essentially constant during the past 20 yr. The 20–25 μm brightness (column labeled 20 μm in Table 1; Fig. 10), which includes the weaker 20 μm silicate feature, shows a decrease comparable to (or somewhat less than) the decrease seen in the 1–7.5 μm continuum over the same time period. There is a considerable difference in the bandpasses in the 20 μm region used by the various photometric systems

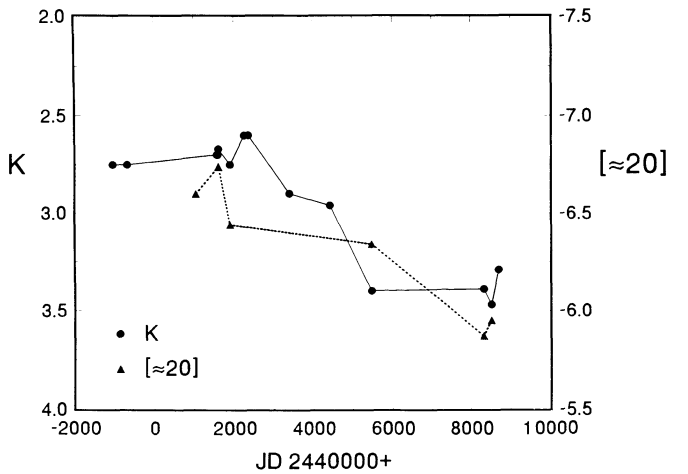

FIG. 10.—Photometric light curve of IRC +10420 from 1965 to 1992 at K (2.2 μm) and in the 20 μm region (column labeled 20 μm in Table 1). Although the bandpasses used for the photometry from 20 to 25 μm are significantly different, there does appear to be a general decline in the 20 μm flux (which includes the 20 μm emission feature) from the 1970s to the present.

referenced in Table 1, so some caution must be used in interpreting the light curve at these wavelengths.

3.5. *Imaging*

The automated plate scanner threshold contours of IRC +10420 illustrated in Figure 3 clearly show that the image is extended in the north-south direction in light polarized at 90°. The north-south elongation seen in light polarized at 90° indicates that the star must have dust at 1″–2″ to the north (or south) that scatters stellar light. Note that, unlike nearby highly polarized reflection nebulae, the entire source is in the 6″ beam of our polarimeters. Therefore, the high intrinsic polarization, several percent in the blue, requires that the scattered light be relatively bright and highly polarized in order for the net polarization of the entire source to be so large. This suggests that the polarization is produced by single scattering, and demands that the scattering dust have a relatively unobscured view of the star, a further indication of a disk type of geometry.

The 8.7 μm image of IRC +10420 is shown in Figure 6. Since the point-spread function for unresolved stars was 2″ FWHM on the night this image was taken, the extension of the image by about 1″ to the northwest is real. Although we have not tried to reconstruct the intrinsic source with a rigorous deconvolution of the image, using simple one-dimensional Gaussians indicates that an intrinsic source extending $\sim$2″ at a position angle of $\sim$150° is consistent with the observed image. In § 4 we will suggest this is the long axis of a disk tilted to the line of sight. Note that the position angle of the calculated intrinsic polarization at 2–3 μm is about 130°–140°, close to the position angle of the elongation in the 8.7 μm image.

4. DISCUSSION

Several lines of evidence lead us to conclude that IRC +10420 is an extremely luminous star near the top of the H-R diagram (Fig. 11) at, or just below, the Humphreys-Davidson limit (Humphreys & Davidson 1979, 1983). The main-sequence progenitor mass must have been at least 40 $M_\odot$. This of course, precludes IRC +10420 from being a proto–planetary nebula in the common definition of the term. We will suggest, however, that IRC +10420 is passing through an analogous phase in its evolution, but at a much higher luminosity. While the structure of its interior is very different from degenerate core giants leaving the AGB, the characteristics of IRC +10420 may have much in common with those of the much less luminous post-AGB giants such as 89 Her and the central star of the Egg Nebula.

In this section we develop a simple semiquantitative model for the structure of the material surrounding IRC +10420 with the assumption that it is a hypergiant. We will concentrate mostly on the optical and infrared observations made to date, but will consider OH maser observations as well. In the final section we speculate on the evolutionary history of this fascinating star.

Several observations discussed in § 3 suggested a disklike structure for some of the material around IRC +10420. The near-infrared continuum (Fig. 4) is very strong, and the overall energy distribution is unlike the twin-peaked "detached-shell" energy distributions typical of proto–planetary nebulae (Hrivnak et al. 1989). The strong 1–5 μm continuum is similar to that found in stars such as MWC 349 (Herzog, Gehrz, & Hackwell 1980), commonly interpreted as due to an optically thick disk with a strong radial temperature gradient. The substantial infrared emission from IRC +10420 requires that a

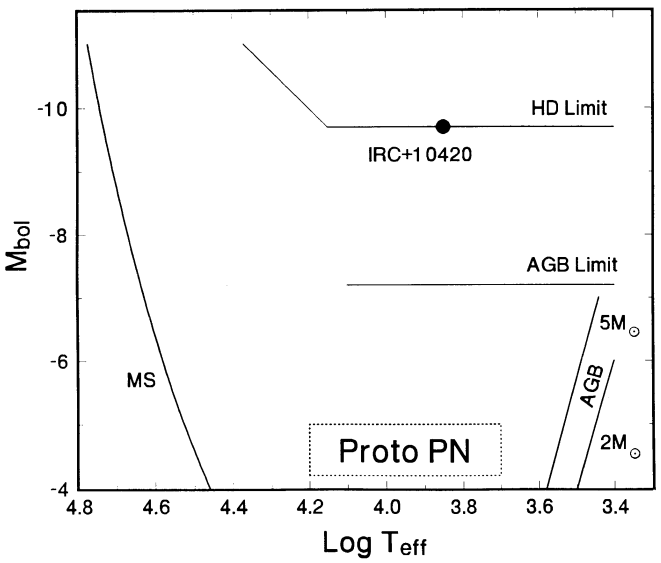

FIG. 11.—Location of IRC +10420 in the H-R diagram compared with degenerate core giants and proto–planetary nebulae. The asymptotic giant branch (AGB) tracks for 2 and 5 $M_\odot$ stars are taken from Bessell et al. (1989). The AGB limit is set by the Chandrasekhar limit for the degenerate core (Paczyński 1970). The location of the proto–planetary nebulae is based on the observed luminosity distribution of the young planetary nebulae (e.g., Pottasch, 1982). The location of the Humphreys-Davidson (HD) limit is taken from Humphreys & Davidson (1979, 1983).

major fraction of the luminosity of the star be absorbed by the surrounding dust, yet we have argued that the reddening is mostly interstellar. We must be viewing IRC +10420 in such a way that the photosphere can be seen through $A_V \sim 1$ mag or less of circumstellar extinction, while in other directions the circumstellar extinction is much greater. A disk, tilted to our line of sight by roughly 45°, allowing the central star to be viewed from out of the plane, will meet this constraint.

The most obvious signature of a rotating disk around IRC +10420 is the double-peaked Hα profile (Fig. 1). The line profile is similar to that found in the classical Be stars, which are universally interpreted as possessing a rotating ionized disk (e.g., Doazan 1982). IRC +10420 is much cooler than the classical Be stars, and although Hα emission is not uncommon in hypergiants, it is unusually strong in IRC +10420. The source of ionization in the disk around the star is unclear, but it probably only affects the innermost volume of the disk inside the dust condensation zone. For a 40 $M_\odot$ star, the observed rotation velocity of the disk ($\sim$55 km s^{-1}) would place the gas causing the emission at a radius of $\sim 2 \times 10^{14}$ cm if the gas were in orbit. This is well inside the 1000 K dust temperature radius of $\sim 2.5 \times 10^{15}$ cm (assuming a 6000 K stellar photosphere and astronomical silicates; Draine 1985).

With the very strong Hα emission (plus Hβ), we should consider the possibility that IRC +10420 may have a hotter companion responsible for the ionization of the hydrogen. The rare [Ca II] emission lines are also relatively strong. These lines have been previously reported in some symbiotic stars and in the peculiar binary υ Sgr, although the nature of the secondary in this system is unknown. Thus, the [Ca II] emission may also be evidence of a companion.

The well-studied cool hypergiant HR 8752 has a hotter, less-luminous companion (B1 main sequence) whose presence is revealed by its contribution to the UV continuum (Stickland & Harmer 1978), a small H II region, and ionization within the

hypergiant's stellar wind (Piters, de Jager, & Nieuwenhuijzen 1988). With the very high interstellar reddening for IRC +10420, the contribution of a less luminous hotter companion to its energy distribution and its spectrum will be much harder to detect. Nevertheless, a hotter, less luminous and less massive companion, presumably still on the main sequence, is an interesting possibility, and it would help explain the presence of an equatorial disk.

The 8.7 μm image of IRC +10420 is clearly elongated (Fig. 6). One-dimensinal speckle interferometry from 2 to 5 μm shows a bright resolved core with an extended large-scale halo surrounding the central source (Dyck et al. 1984; Ridgway et al. 1986; Cobb & Fix 1987). The core has a diameter of about 0".22 at 2.2 μm (1.6×10^{16} cm at 5 kpc). The halo is about 1"–1".5 in diameter and contributes 10%–20% of the total emission at 2.2 μm. There is no clear north-south–east-west asymmetry in the near-infrared speckle observations, although the north-south and east-west one-dimensional scans at 2.2 μm will not detect any asymmetry in an image extended along a position angle of 45° or 135°. One-dimensional speckle interferometry in the 10 μm band also shows a resolved source (Cobb & Fix 1987; Fix & Cobb 1988). Cobb & Fix (1987) find that the high spatial frequency data at 10 μm imply a double source or ring structure with a separation of 0".7 oriented at either 40° or 140°. Within the errors, this is consistent with the position angle of ~150° for the elongation seen in our 8.7 μm image. Fix & Cobb (1988) find no difference between the angular size at 8.7 and 9.7 μm. This suggests a different geometry than a spherical dust shell where the angular size in the silicate feature (9.7 μm) is expected to be larger (e.g., Cobb & Fix 1987). Also, they were unable to model their speckle results using a spherical, optically thin dust shell.

There is clear evidence that both the tilted disk and the more extended circumstellar environment around IRC +10420 have undergone considerable changes in this century. The most conspicuous aspects of the photometric changes (§ 3.4) seen in IRC +10420 are the steady brightening in B by 1 mag over several decades up to 1970 and the subsequent decrease in the 1–7.5 μm continuum during the 1980s. Whether the two are related is an interesting question. The drop in the near-infrared continuum is strongly suggestive of a clearing of dust out of the hotter inner portions of the circumstellar disk around the star. If this clearing began earlier in the century, it could explain the brightening in the visual. In other words, IRC +10420 has been removing dust from the inner portions of its circumstellar environment for the past several decades. As the dust begins clearing, the amount of circumstellar extinction to the star along our line of sight is reduced and the star brightens in the visual. This initial clearing affects primarily the extinction to the star as viewed from the Earth, not the near-infrared continuum. As the process continues, the optically thick portions of the circumstellar disk begin to dissipate and the near-infrared continuum drops in intensity. Most of the extinction is now interstellar, and any modest circumstellar extinction along our line of sight is probably outside the volume affected by this hypothesized clearing process. Note that the polarization has also changed between the two epochs for which we have data. Clearly there have been significant changes in the geometry of the dust around IRC +10420.

IRC +10420 has the silicate features at 10 and 20 μm strongly in emission. The ratio of the strength of the two features is unusual in that the 20 μm feature is stronger relative to the 10 μm feature than is typical for stars with dusty circumstellar shells (Rowan-Robinson & Harris 1983). This fact led Fix & Cobb (1988) to speculate that IRC +10420 contained peculiar dust grains, although it is more likely that the 10 μm feature is partially self-absorbed. If this were the case, a clearing of dust would reduce the emission at all wavelengths except in the middle of the silicate feature at 10 μm. At that wavelength the reduced exit optical depth could compensate for the reduction in available dust.

At the distance and luminosity of IRC +10420, the inner edge of the dust in the circumstellar disk will be located at a radius of about 2.5×10^{15} cm (assuming normal silicates and $T_{\rm dust} \sim 1000$ K). For a 40 $M_\odot$ star, the orbital time at this radius is about 10^2 yr. The outflow velocity observed in the OH maser emission (which is at larger radii) is about 25 km s^{-1}. For simple radial outflow, this velocity yields a moderately shorter dynamical time for changes at the inner dust radius. Thus, the changes seen in the inner portions of the material surrounding IRC +10420 are taking place on a time scale comparable to that of orbital motion or the mass-loss wind. This suggests that changes in the physical conditions above the photosphere of the star have caused a clearing of dust from at least the inner portions of the disk. The location of the high-velocity wind is not clear, but it probably occupies a more extensive volume than the disk, perhaps a fast, low-density polar outflow.

Alternatively, the brightening could have been due to an increase in the intrinsic luminosity of the star that would then have moved the grain condensation/destruction boundary further out. The time scale for grain destruction is not well established in cool variable stars, but it is probably considerably shorter (see Suh, Jones, & Bowen 1990) than the several decades IRC +10420 spent brightening in the visual. Also, while the hypergiants are observed to vary in spectral type, they tend to remain at a constant total luminosity during these variations (Humphreys 1988, 1983).

A schematic diagram of our model is shown in Figure 12. Some features of the model are quantitative and some are qualitative. This model explicitly assumes that IRC +10420 is

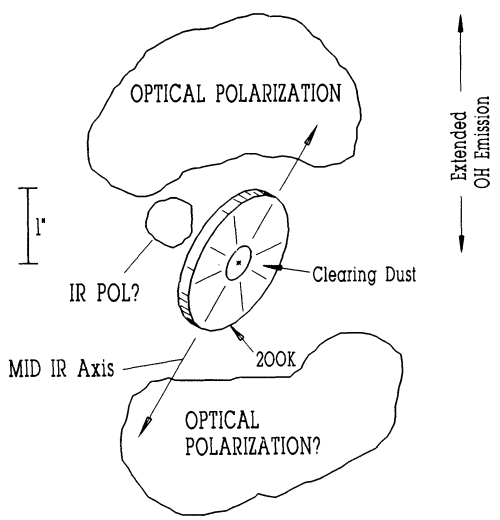

FIG. 12.—Suggested geometry for IRC +10420 and its immediate environment. The diagram is drawn as the system is seen in the plane of the sky, with north at the top. The extended dust clouds and the outer contour of the equatorial disk are drawn to scale. The inner contour of the disk is exaggerated in size for clarity.

at 5 kpc from the Sun and has an intrinsic luminosity of $6 \times 10^5\ L_\odot$. The location of the 200 K dust temperature contour in the disk is drawn to scale. Most of the 10 and 20 μm light will come from within the contour. (For clarity the 1000 K dust temperature contour is shown at a larger radius than it should be.) Note that the angular size of the 200 K contour is comparable to the angular size necessary to explain the 8.7 μm image. The tilt of the disk is not well constrained. The high polarization and the elongated 8.7 μm image indicate that it cannot be face-on, while the lack of high circumstellar extinction indicates that it cannot be edge-on either.

The position angle of the intrinsic polarization in the optical is about 100° (§ 3.2), which is significantly different from the 140°–150° position angle of the disk as inferred from the 8.7 μm image and the 10 μm speckle interferometry. The very high polarizations often seen in bipolar nebulae are in part due to unpolarized light from the central star being blocked by an edge-on circumstellar disk. Since the light from the photosphere of IRC +10420 is only partly obscured, the high intrinsic polarization in the blue (Fig. 8) requires that the scattering dust subtend a substantial solid angle around the star. In our schematic model of the circumstellar environment around IRC +10420 we have placed the dust causing the optical polarization in an extensive region north of the star where considerable OH maser emission is found (Bowers 1984). The maser emission is an indicator of the presence of circumstellar material at that location. We have also placed dust symmetrically south of the star, even though there is no maser emission from that location. This will help to provide as large a solid angle for dust scattering as possible. Note that the geometry does *not* conform to a classic bipolar nebula with symmetric scattering lobes directly above and below the plane of the circumstellar disk. Our observations suggest that the dust around IRC +10420 is very patchy and complex. The location of the scattering may be more a function of how the dust is illuminated—through holes in the circumstellar extinction, for example—than of the actual density distribution in the circumstellar environment.

The calculated intrinsic infrared polarization has a position angle of ~130°–140° (Fig. 8), which is significantly different from the position angle in the visual. This is unusual for stars with circumstellar dust shells but is not unique to IRC +10420. WX Ser (a dusty Mira) and HM Sge (a symbiotic proto–planetary nebula), for example, show a similar strong rotation in position angle in their intrinsic polarization (McCall & Hough 1980; Johnson & Jones 1991). The explanation for HM Sge devised by Johnson & Jones (1991) can be applied in broad terms here as well. Basically, the region producing the near-infrared polarization is sufficiently optically thick that optical photons cannot penetrate the region easily and are also multiply scattered. The infrared light penetrates farther and is mostly singly scattered and hence produces more polarized intensity. The near-coincidence of the position angle for the infrared polarization and the angle of the tilted disk is suggestive. Perhaps the dust causing the infrared polarization is located in dense clumps above the plane of the disk. Wherever it is located, it must not significantly block light from the star reaching the scattering dust grains that produce the optical polarization. Note that the intrinsic infrared polarization is relatively weak and does not place strong constraints on the model.

In our model we have not explicitly located the OH masing regions. The spatial distribution of the OH maser emission is very complex and a strong function of the velocity of the emission (Nedoluha & Bowers 1992). The maser emission has been variously described as a spherically expanding shell (Bowers 1984), a bipolar outflow seen face-on (Diamond et al. 1983), and a complex mixture of spherical outflow and extensive clumping (Nedoluha & Bowers 1992). Our model does not directly address the geometry of the OH maser emission, but it does contain elements of all three geometries. According to Bowers (1984), the central star in IRC +10420 is located at the same position as the spatially compact southern maser emission that spans velocities from 40 to 60 km s^{-1}. This emission is blueshifted relative to the velocity of the star (76 km s^{-1}; § 3.1) and may be traveling toward us out from the star, perhaps along the pole of the disk. Diamond et al. (1983) suggested that this emission is part of a bipolar flow viewed from above one of the poles. Our geometry does not preclude a bipolar flow, but it must be viewed at an angle well off the pole.

The much weaker OH maser emission at 100–104 km s^{-1} extends up to 4″ to the north of the star (Bowers 1984) and covers several square arcseconds on the sky. This emission is redshifted relative to the star, and may be traveling out the opposite pole of the disk away from us. We tentatively associated this emission with the dust causing the optical polarization. There could also be dusty material to the south scattering light, but it does not produce maser emission. At the distance of IRC +10420, the OH emission 4″ to the north is at a distance of 3×10^{17} cm from the star. At an expansion velocity of 25 km s^{-1} (half the observed velocity spread of the maser emission), it would take about 4000 yr to reach this distance from the star. This is comparable to the time it would take a massive star to evolve from a red supergiant to an F-type hypergiant, suggesting that this dust and gas may have been lost in a previous phase of evolution (Mutel et al. 1979). The high-velocity wind seen in the wings of Hα is probably a more recent phenomenon.

Finally, we consider the change in the relative strengths of the 1665 and 1612 MHz OH lines reported by Lewis et al. (1986). In general, stellar masers with very thin dust shells show main-line emission at 1665 MHz and little or no satellite emission at 1612 MHz. In type II masers with optically thick dust shells, however, the 1612 MHz line dominates. IRC +10420 shows strong emission at both 1612 and 1655 MHz, but Lewis et al. observed that the strongest feature in the 1612 MHz emission increased in intensity by a factor of 3 between 1982 and 1985, while the emission at 1665 MHz decreased. Using the model for OH emission presented by Field (1985), Lewis et al. suggest that the column depth of the masing region has increased, causing the saturated 1612 MHz maser to increase at the expense of the 1665 MHz feature. This explanation would suggest an increase in the dust around the star, apparently in conflict with our conclusion that the dust is actually being dispersed. This discrepancy is easily explained, however, by the fact that the maser emission is at much greater distances (~10^{16}–10^{17} cm) from the star than the hot inner portions of the disk (~10^{15} cm). The changes in the geometry, density, and motions of the material in the OH masing region is more a function of the mass-loss history stretching back a thousand years or more than of recent events closer to the star. Changes in the illumination of the diffuse material, and therefore in the strength of the 35 μm pump, could be tied to more recent events close to the star.

5. CONCLUSIONS

In the previous sections we have presented strong arguments in favor of placing IRC +10420 at 4–6 kpc from the Sun,

TABLE 5

COMPARISON OF IRC +10420 WITH DUSTY LATE AGB STARS AND PROTO-PLANETARY NEBULAE

Property	IRC +10420	Dusty Late AGB	Edge-on Proto-Planetary Nebulae
Luminosity ($L_\odot$)	5×10^5	10^4	10^4
Spectral type	F Ia+	Late M III	(A–G) I
MS mass ($M_\odot$)	40	2–8	2–8
Silicates	Emission	Absorption	Weak or absent
OH maser	Yes	Yes	Rare
Polarization	8%	1%–5%	10%–40%
Hα emission	Strong, broad	Weak, none	Narrow
Disk	Yes	Probably	Yes

making the star a true core-burning supergiant near the top of the H-R diagram. The numerous and diverse observations of IRC +10420 presented in this paper indicate a very rich and complex circumstellar environment for the star. Central to our conclusions is the presence of an equatorial disk of gas and dust, tilted to our line of sight and surrounded by a more diffuse and clumpy distribution of gas and dust. Changes in the brightness of the star from the 1930s to the present are explained by the dissipation of dust from the inner portions of its circumstellar environment. This dissipation first cleared along out line of sight to the Sun, causing the star to brighten in the visual from 1926–1927 to 1970. Continued dissipation of dust in the denser tilted disk has caused the infrared continuum to drop from 1972 to 1985.

The star and its equatorial disk are surrounded by a complex, clumpy, and more diffuse distribution of gas and dust. This more diffuse material gives rise to the OH maser emission and contributes the major fraction of the intrinsic polarization. The location of the scattering may be more a function of how the dust is illuminated—through holes in the circumstellar extinction, for example—than of the actual density distribution of the more diffuse material. Changes in the relative strengths of the 1612 and 1665 MHz OH maser emission that took place in the mid-1980s have been interpreted (Lewis et al. 1986) as an increase in the column length of the masing region, apparently in conflict with our conclusion that the star is dispersing dust. The diffuse material surrounding the star, however, took several thousand years to reach its current extent. The changes in the geometry and motions of the material in the OH masing region is more a function of the mass-loss history stretching back a thousand years or more than of recent events closer to the star. Changes in the illumination of the more extensive circumstellar material could, however, be significantly influenced by events closer to the star.

Because of the presence of OH maser emission and substantial dust at large distances from IRC +10420, it is tempting to associate this material with mass lost during a preceding red supergiant phase. Mutel et al. (1979) speculated that the extensive dust shell around IRC +10420 formed in the preceding red supergiant phase and that the mass loss has stopped, leaving the remaining fossil shell to dissipate with time. The presence of an equatorial disk and the strong near-infrared continuum clearly indicate that there is still considerable material in close proximity to the star. This suggests that mass loss is still taking place at a substantial rate, perhaps as high as the $(1–5) \times 10^{-4}\ M_\odot\ \mathrm{yr}^{-1}$ determined from observations of the more diffuse material surrounding the star. Since extremely luminous stars in the yellow and red portions of the H-R diagram evolve on very rapid time scales, the complex circumstellar environment of IRC +10420 presents us with a "snapshot" of its mass-loss history through more than one phase of the star's evolution.

Consider a star that beings its life on the main sequence with 40 $M_\odot$. By the time it becomes a red supergiant it will have lost $\sim 8\ M_\odot$, based on the models by Maeder & Meynet (1988). Using their models and the mass-loss compilation by de Jager, Nieuwenhuijzen, & van der Hucht (1988), we find that as a normal red supergiant it will lose another solar mass ($M \sim 3 \times 10^{-5}\ M_\odot\ \mathrm{yr}^{-1}$ for 4×10^4 yr), and in the OH/IR star phase it will lose about 5 $M_\odot$ ($M \sim 5 \times 10^{-4}\ M_\odot\ \mathrm{yr}^{-1}$ for 1×10^4 yr). The star will then evolve to the blue in the H-R diagram, spending about 4×10^4 yr as an F–K hypergiant. If the mass loss continues at $\sim 10^4\ M_\odot\ \mathrm{yr}^{-1}$, it will lose another 4 $M_\odot$. When the star, initially 40 $M_\odot$, leaves the F hypergiant stage, it will have only 20 $M_\odot$ left. In essence, a major fraction of the hydrogen-rich envelope of the star has been lost. According to models by Maeder & Meynet (1988), the relative surface abundance of hydrogen will be down to 0.2, leaving the star with a helium-rich envelope. If the star continues to evolve to hotter temperatures, it will very likely become a Wolf-Rayet star. If the cumulative mass loss is not as high as we have estimated, IRC +10420 may become a blue supergiant and go supernova before losing its hydrogen envelope.

Although not a degenerate core giant, IRC +10420 presents us with many parallels to the evolution of red giants from the upper asymptotic giant branch through the proto–planetary nebula stage to the central star of a planetary nebula (Table 5). Cool, luminous AGB stars go through a high mass loss phase and develop into OH/IR stars before evolving into proto–planetary nebulae. Continued mass loss quickly strips the remaining hydrogen-rich envelope from the star and bares the hot degenerate core. Like many of the proto–planetary nebulae, IRC +10420 displays strong intrinsic polarization, contains the remnants of the mass-loss wind from the OH/IR star phase, and shows evidence for a dusty disk surrounding the star. Unlike the proto–planetary nebulae, the much more massive and luminous IRC +10420 will not evolve into the central star of a planetary nebula. As the remaining hydrogen-rich envelope is lost and interior layers are exposed, IRC +10420 will likely evolve into a Wolf-Rayet star.

We thank Ed Ney for letting us make use of his Schmidt plates. This research has been supported in part by grants from NSF, NASA, and the Graduate School of the University of Minnesota.

REFERENCES

Andrillat, Y. 1982, in IAU Colloq. 70, The Nature of Symbiotic Stars, ed. M. Friedjung & R. Viotti (Boston: Reidel)
Atlas of Low Resolution *IRAS* Spectra. 1986, *IRAS* Science Team, prepared by F. M. Olnon & E. Raimond, A&AS, 65, 607
Bessell, M. S., Brett, J. M., Scholz, M., & Wood, P. R. 1989, A&A, 77, 1
Bowers, P. F. 1984, ApJ, 279, 350
Bowers, P. F., & Knapp, G. R. 1989, ApJ, 347, 325
Clemens, D. P. 1985, ApJ, 295, 422
Cobb, M. L., & Fix, J. D. 1987, ApJ, 315, 325
Craine, E. R., Schuster, W. J., Tapia, S., & Vrba, F. J. 1976, ApJ, 205, 802
de Jager, C. Nieuwenhuijzen, H., & van der Hucht, K. A. 1988, A&AS, 72, 259
Diamond, P. J., Norris, R. P., & Booth, R. S. 1983, A&A, 124, L4
Doazan, V. 1982, in B Stars with and without Emission Lines (NASA SP-456), 279
Draine, B. T. 1985, ApJS, 57, 587
Dyck, H. M., Forbes, F. F., & Shawl, S. J. 1971, AJ, 76, 901
Dyck, H. M., Zuckerman, B., Leinert, Ch., & Beckwith, S. 1984, ApJ, 287, 801
Field, D. 1985, MNRAS, 217, 1
Fix, J. D. 1981, ApJ, 248, 542
Fix, J. D., & Cobb, M. L. 1987, ApJ, 312, 290
———. 1988, ApJ, 329, 290
Forrest, W. J., McCarthy, J. F., & Houck, J. R. 1979, ApJ, 233, 611
Gehrz, R. D., Grasdalen, G. L., Hackwell, J. A. 1987, in Encyclopedia of Physical Science and Technology, 2 (New York: Academic), 53
Gehrz, R. D., & Hackwell, J. A. 1978, S&T, 55, 466
Gehrz, R. D., Hackwell, J. A., & Jones, T. W. 1974, ApJ, 191, 675
Giguere, P. T., Woolf, N. J., & Weber, J. C. 1976, ApJ, 207, L195
Glaccum, W. J., Moseley, S. H., Campins, H., & Loewenstein, R. F. 1987, A&A, 187, 635
Gottlieb, E. W., & Liller, W. 1978, ApJ, 225, 488
Grasdalen, G. L., Gehrz, R. D., Hackwell, J. A., Castelaz, M., & Gullixson, C. 1983, ApJS, 53, 413
Habing, H. J., Hekkert, P., & van der Veen, W. E. C. J. 1989, in IAU Symp. 131, Planetary Nebulae, ed. S. Torres-Peimbert (Dordrecht: Reidel), 381
Hanner, M. S., Newburn, R. L., Gehrz, R. D., Harrison, A. T., & Ney, E. P. 1990, ApJ, 348, 312
Herzog, A. D., Gehrz, R. D., & Hackwell, J. A. 1980, ApJ, 236, 189
Hrivnak, B. J., Kwok, S., & Volk, K. M. 1989, ApJ, 346, 265
Humphreys, R. M., 1983, ApJ, 269, 335
———. 1988, in ASP Conf. Ser., Vol. 4, ASP Symposium on the Extragalactic Distance Scale (San Francisco: ASP), 103
Humphreys, R. M., & Davidson, K. 1979, ApJ, 232, 409
———. 1983, Science, 223, 243
Humphreys, R. M., Strecker, D. W. Murdock, T. L., & Low, F. J. 1973, ApJ, 179, L49
Humphreys, R. M., Jones, T. J., & Sitko, M. L. 1984, AJ, 89, 1155
IRAS Point Source Catalog, Version 2. 1988, Joint *IRAS* Science Working Group (Washington, DC: GPO)
Johnson, J. J., & Jones, T. J. 1991, AJ, 101, 1735
Jones, T. J., & Gehrz, R. D. 1990, AJ, 100, 274
Jones, T. J., & Klebe, D. I. 1988, PASP, 100, 1158
Knapp, G. R., & Morris, M. 1985, ApJ, 292, 640
Landolt, A. U. 1983, AJ, 88, 439
Lawrence, G., Jones, T. J., & Gehrz, R. D. 1990, AJ, 99, 1232
Lee, T. A. 1972, private communication
Lewis, B. M., Terzian, Y., & Eder, J. 1986, AJ, 302, L23
Maeder, A., & Meynet, G. 1988, A&AS, 76, 411
McCall, A., & Hough, J. H. 1980, A&AS, 42, 141
Merrill, P. W. 1943, PASP, 55, 242
Mutel, R. L., Fix, J. D., Benson, J. M., & Webber, J. C. 1979, ApJ, 228, 771
Nedoluha, G. E., & Bowers, P. F. 1992, ApJ, 392, 249
Neugebauer, G., & Leighton, R. B. 1969, Two Micron Sky Survey: A Preliminary Catalog (NASA SP-3047)
Ney, E. P. 1974, ApJ, 189, L141
Ney, E. P., & Merrill, K. M. 1980, Study of Sources in AFGL Rocket Infrared Survey (AFGL-TR-80-0050)
Omont, A., Moseley, S. H., Forveille, T., Glaccum, W. J., Harvey, P. M., Likkel L., Lowenstein, R. F., & Lisse, C. M. 1990, ApJ, 355, L27
Osmer, P. S. 1972a, ApJ, 171, 393
———. 1972b, ApJS, 24, 247
Paczyński, B. 1970, Acta Astron., 20, 47
Peterson, D. M. 1992, private communication
Piters, A., de Jager, C., & Niewenhuijzen, H. 1988, A&A, 196, 115
Pottasch, S. R. 1982, in IAU Symp. 103, Planetary Nebulae, ed. D. R. Flower (Boston: Reidel), 391
Reid, M. J., Moran, J. M., Leach, R. W., Ball, J. A., Johnston, K. J., Spencer, J. H., & Swenson, G. W. 1979, ApJ, 227, L89
Ridgway, S. T., Joyce, R. R., Connors, D., Pipher, J. L., & Dainty, C. 1986, ApJ, 302, 662
Rowan-Robinson, M., & Harris, S. 1983, MNRAS, 202, 767
Serkowski, K., Mathewson, D. S., & Ford, V. L. 1975, ApJ, 196, 261
Sitko, M. L., Schmidt, G. D., & Stein, W. A. 1985, ApJS, 59, 323
Slovik D. J., & Peterson, D. M. 1992, BAAS, 24, 801
Stickland, D. J., & Harmer, D. L. 1978, A&A, 70, L53
Suh, K-W., Jones, T. J., & Bowen, G. H. 1990, ApJ, 358, 588
Thomas, J. A., Robinson, G., & Hyland, A. R. 1976, MNRAS, 174, 711
Walker, R. G., & Price, S. D. 1975, AFGL Infrared Sky Survey (AFGL-TR-75-0373)
Wilking, B. A., Lebofsky, M. J., Martin, P. G., Rieke, G. H., & Kemp, J. C. 1980, ApJ, 235, 905
Zickgraf, F.-J., Wolf, B., Stahl, O., Leitherer, C., & Appenzeller, I. 1986, A&A, 163, 119
Zickgraf, F.-J., Wolf, B., Stahl, O., Leitherer, C., & Klare, G. 1985, A&A, 143, 421